International Conference on Modelling and Control of Joining Processes, Orlando, Florida (1993), ed T. Zacharia, American Welding Society, pp. 153–160.

MODEL FOR BORON EFFECTS IN STEEL WELDS

H. K. D. H. Bhadeshia* and L.–E. Svensson †

ABSTRACT

Boron is often used as a trace addition in steel welds to control the formation of phases which initiate at the austenite grain surfaces. This work deals with a quantitative model for the effect of boron on the development of microstructure in steel welds as they cool after solidification. The theory is compared with experimental data and found to give reasonable agreement.

INTRODUCTION

It is well established that boron increases the bainitic hardenability of steels by retarding the heterogeneous nucleation of ferrite at the austenite grain surfaces (Ref. 1). It is probable that this effect is due to the reduction in interfacial energy as the boron segregates to the boundaries. This in turn makes grain boundaries less effective as heterogeneous nucleation sites. For typical commercial steels, a soluble boron concentration of $\simeq 0.002$ wt.% is often sufficient, although the exact amount must depend on the amount of austenite grain surface per unit volume. Too large an addition is detrimental because it leads to the formation of borides at the austenite grain boundaries and these are known to *enhance* the nucleation of ferrite (Ref. 2). Boron is also ineffective as an oxide or nitride. The purpose of this work was to develop an existing model for the prediction of microstructure in the fusion zone of steel welds, to incorporate the effects of trace additions of boron.

SOLUBILITY OF BORON IN AUSTENITE

The amount of nitrogen that is left after reaction with titanium, x_N^{Ti} is calculated as described elsewhere (Ref. 3). Fountain and Chipman (Ref. 4) have given a solubility product for the reaction in austenite,

$$\mathrm{B} + \mathrm{N} \rightleftharpoons \mathrm{BN} \tag{1}$$

$$\log\{x_B^S x_N^S\} = -\frac{13970}{T} + 5.24 \tag{2}$$

where x_B^S and x_N^S are the dissolved boron and nitrogen concentrations (in wt.%) respectively, and T is the absolute temperature. For a specified temperature, there are therefore two unknowns. The problem was solved iteratively by at first setting the soluble nitrogen concentration to the total that is available after reacting with titanium:

$${}_1x_N^S = x_N^{Ti} \qquad \text{first iteration} \tag{3}$$

This gave a first estimate ${}_1x_B^S$ of the soluble boron; the nitrogen tied up with boron could then be calculated. The amount of nitrogen left after reaction with titanium and boron, $x_N^{Ti,B}$ is therefore obtained as a residue. In the second iteration, the soluble nitrogen is set equal to this residue:

$${}_2x_N^S = x_N^{Ti,B} \qquad \text{second iteration} \tag{4}$$

† ESAB AB, Sweden; *Cambridge University/JRDC, U.K.

This gives a new value for x_B^S and the process is repeated until the value converges. At that instant, we obtain both the nitrogen and boron concentrations in solution in the austenite, and hence also the amount of boron x_B^{BN} that is tied up as BN by taking the difference $x_B^{BN} = x_B - x_B^S$, x_B being the total concentration of boron.

Throughout these calculations, the temperature at which the solubility of boron in austenite was evaluated was fixed at 940 °C, which is about 30 °C above that at which pure iron transforms to ferrite (some elements such as silicon can raise this equilibrium temperature). There clearly is uncertainty in choosing an appropriate temperature, and there is an implicit assumption that the boron always is at equilibrium in the austenite as it cools to 940 °C. These approximations may not lead to large errors in the present context, because as will be seen later, the limiting concentration beyond which dissolved boron has no further effect, is rather small when compared with typical additions that are made in steel welds. However, this is an area for further work.

CALCULATION OF TTT DIAGRAM

A time–temperature–transformation (TTT) diagram consists essentially of two C–curves (Ref. 5), the one at higher temperatures representing reconstructive transformation to ferrite or pearlite, and that at lower temperatures where atomic mobility is diminished, representing displacive transformations such as Widmanstätten ferrite, bainite and acicular ferrite. Boron has the largest effect on the C–curve for reconstructive transformations (Fig. 1a), leaving the lower C–curve hardly changed. The increase in the incubation period ($\Delta\tau$) before reconstructive transformation begins, as a function of the soluble boron concentration has been investigated quantitatively by Pickering (Ref. 2, Fig. 1b). There is a proportional increase in the incubation period until a concentration of about 20 p.p.m. is reached, after which the function becomes insensitive to boron and the overall effect becomes unreliable.

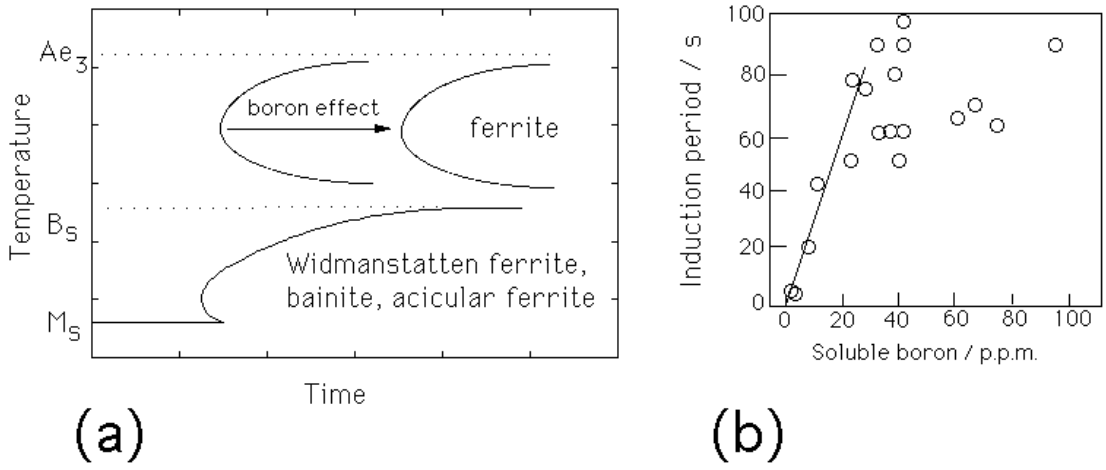

Fig. 1: (a) The effect of boron and its analogues (the rare earth elements) on the TTT diagram, showing a pronounced effect on the allotriomorphic ferrite transformation but only a minor retardation of bainitic reaction. (b) Change in the incubation time for the allotriomorphic ferrite reaction as a function of the soluble boron concentration (Ref. 2)

For the present work, Pickering's data are represented as follows:

$$\Delta\tau = x_B^S \times 3.4 \qquad \text{for} \qquad x_B^S \leq x_B^C \tag{5}$$

where $\Delta\tau$ has units of seconds, and x_B^S is the concentration of dissolved boron in parts per million by weight. The term x_B^C is a critical concentration beyond which a further enhancement in the soluble boron concentration does not increase hardenability. Presumably because of the large austenite grain size found in welds, this limiting concentration was found by comparison with experimental data described later, to be only 3 p.p.m. ($x_B^C = 3$), so that

$$\Delta\tau = 10.2 \qquad \text{for} \qquad x_B^S \geq x_B^C \tag{6}$$

Using an established model (Ref. 6) for the calculation of the TTT diagram for multicomponent steels, it becomes simple to include the effect of boron, by retarding the reconstructive C–curve at all temperatures by $\Delta\tau$. This was incorporated into our model for the prediction of microstructure in the fusion zone of steel welds (Ref. 3).

COMPARISON WITH EXPERIMENTAL DATA

The weld metal data used to test and calibrate the model are from Ref. 7, where the microstructures of boron containing welds were examined in detail. They were manual metal arc welds deposited using 4 mm electrodes with an ISO2560 all–weld metal joint preparation in 20 mm thick plates. The electrodes were used with DC+ 24 V, 180–195 Amps current and 240 °C interpass temperature. The chemical compositions and the microstructures obtained are summarised in Tables 1 and 2. The nitrogen and oxygen levels do not vary significantly and represent the mean values typical of such welds. The metallographic data reported in Table 2 have been measured for the as–deposited microstructure, V_α, V_w and V_a representing the volume fractions of allotriomorphic, Widmanstätten and acicular ferrite respectively. $\overline{L}_{tn}$ is a measure of the columnar austenite grain size, as discussed in Ref. 3.

Weld	C	Si	Mn	B	N	O	Al	Ti
1	0.044	0.37	1.03	**0.0001**	0.007	0.0035	0.011	0.025
2	0.046	0.37	1.05	**0.0020**	0.007	0.0035	0.010	0.024
3	0.044	0.36	0.99	**0.0020**	0.007	0.0035	0.010	0.023
4	0.044	0.44	1.06	**0.0052**	0.007	0.0035	0.010	0.027
5	0.044	0.44	1.06	**0.0065**	0.007	0.0035	0.012	0.027

Table 1: Chemical composition, wt.%

Weld	V_α	V_w	V_a	$\overline{L}_{tn}$, μm
1	0.42	0.29	0.29	146
2	0.40	0.12	0.48	126
3	0.33	0.03	0.64	131
4	0.37	0.00	0.63	112
5	0.34	0.00	0.66	123

Table 2: Microstructural data (Ref. 7)

The data in Table 2 are interesting in two respects. As expected, there is a monotonic decrease in the allotriomorphic ferrite content as the boron concentration is increased. Weld 2 has a large V_α even though it has the same boron concentration as Weld 3, but this is because of its smaller austenite grain size, an effect which is accounted for in the modelling (Ref. 3). Hence, the modification of the model to incorporate a retardation of the upper C–curve of the TTT diagram should be sufficient to predict variations in V_α as a function of boron.

The second observation from Table 2 is that the amount of Widmanstätten ferrite is also reduced quite significantly by boron. This can be understood once it is realised that most of the Widmanstätten ferrite in welds nucleates at allotriomorphic ferrite/austenite interfaces, as illustrated in Fig. 2. Allotriomorphic ferrite usually nucleates at the austenite grain boundary, and has an appropriate orientation relationship with only one of the adjacent austenite grains (Ref. 8). Widmanstätten ferrite, due to its mechanism of transformation, can only nucleate from allotriomorphic ferrite into that austenite grain (Ref. 9). Boron reduces the number of allotriomorphs, so that the few that are nucleated spread along boundaries where they are not appropriately orientated with either of the adjacent austenite grains, and hence cannot develop into Widmanstätten ferrite, (Fig. 2). To take account of this effect, it is necessary to suppress the formation of Widmanstätten ferrite in the presence of boron. This has been done by multiplying the fraction V_w as calculated in the absence of boron, by a factor of 0.2 in order to match the experimental data.

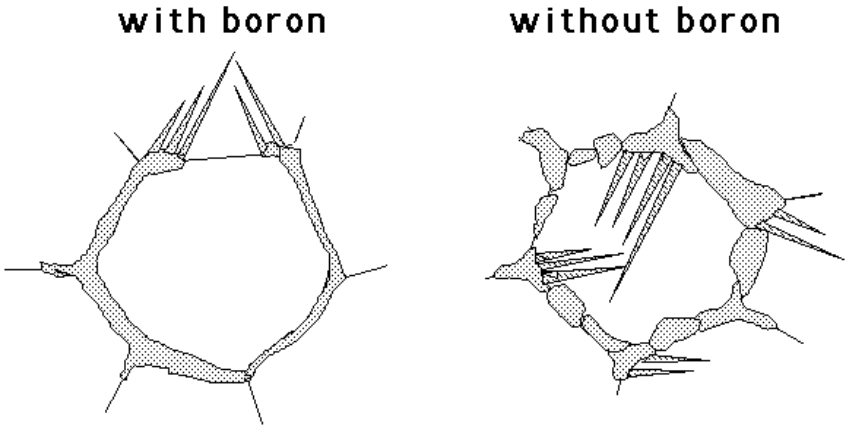

Fig. 2: Formation of Widmanstätten ferrite from allotriomorphic ferrite.

Temperature used for solubility product in γ	940 °C
Slope of $\Delta\tau$ vs x_B^S line	3.4 s p.p.m^{-1}
Limiting B concentration x_B^C	3 p.p.m.
Factor by which V_w is multiplied	0.2

Table 3: Calibration factors for the boron effect

The variety of approximations used in order to incorporate the boron effect have already been presented in the text, but are highlighted again in Table 3. A comparison between the experimental data and calculations using our model modified to include the boron effect is presented in Fig. 3 – the agreement is good. A further comparison with the experimental data

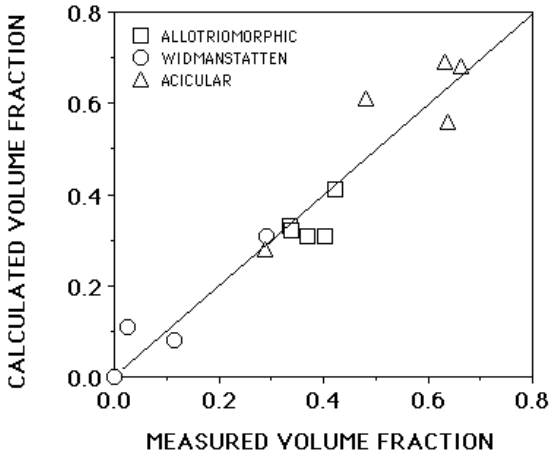

Fig. 3: Comparison between experiment (Ref. 7) and theory

Weld	Calculated			Experimental		
	V_α	V_w	V_a	V_α	V_w	V_a
K8	0.09	0.02	0.89	0.10	0.00	0.90
K9	0.10	0.03	0.87	0.09	0.00	0.91
K10	0.07	0.02	0.91	0.08	0.00	0.92
B1,B2,B3,B4	0.00	0.00	1.00	0.00	0.00	1.00

Table 4: Calculated and Experimental (Ref. 10) data for B welds

of Snieder and Kerr (Ref. 10) for completely different welds (submerged arc, multicomponent) shows again that the method used is reasonable (Table 4).

We now illustrate the modified model. An important point is that boron must be protected against nitrogen. The trace element concentrations (Al, Ti, N, O) have to be chosen carefully; otherwise the titanium is unable to protect boron against the nitrogen. The methodology for that has been discussed elsewhere (Ref. 3) and is not described here. The calculations are illustrated in Table 5 and Fig. 4. From Table 5, we note that weld (a) is free of boron, (b) has 20 p.p.m. of boron which is inadequately protected by Ti (which combines with oxygen, leaving the N unaffected), (c) contains a larger concentration of Ti, so that the soluble boron concentration is increased, and (d) contains a lower Ti but larger boron concentration to achieve an enhanced soluble boron concentration. In practice, route (c) is better than (d) because boron becomes unreliable at large concentrations.

SUMMARY

A model for the calculation of the primary microstructure of multicomponent steel welds has been modified to incorporate the effects of trace additions of boron. The method allows for a retardation of the upper C–curve of the time–temperature–transformation diagram as a function of the soluble boron concentration. An interesting outcome is that boron also has a large tendency to suppress the formation of secondary Widmanstätten ferrite, and this will form the subject of future more fundamental studies. The model gives reasonable agreement with experimental data.

Example	Ti as Ti_2O_3	Ti as TiN	Dissolved B	B as BN	Dissolved N
(a) 0 B, 270 Ti	270	0	0	0	79
(b) 20 B, 270 Ti	270	0	1.0	19.0	54
(c) 20 B, 450 Ti	368	82	1.7	18.3	31
(d) 40 B, 270 Ti	270	0	1.9	38.1	30

Table 5: Calculated trace element data for welds with 300 O, 79 N, 150 Al. The concentrations are all in p.p.m. by weight.

The authors are grateful to Professor C. J. Humphreys and ESAB AB (Sweden) for the provision of laboratory facilities. HKDHB's contribution was via the "Atomic Arrangements: Design and Control Project", which is a collaborative effort between the University of Cambridge and the Research and Development Corporation of Japan.

REFERENCES

1. Banerji, S. K.; and Morral, J. E., eds. 1980. Conference Proceedings. Boron in Steel TMS–AIME, Warrendale, PA, USA, 1–215.
2. Pickering, F. B. 1978. Physical Metallurgy and the Design of Steels App. Sci., UK.
3. Bhadeshia, H. K. D. H.; and Svensson, L.–E. 1993. Modelling the evolution of microstructure in steel weld metal. Mathematical Modelling of Weld Phenomena eds. H. Cerjak and K. E. Easterling, Institute of Materials 109–182.
4. Fountain, W.; and Chipman, J. 1962. Solubility and precipitation of boron nitride in Fe–B alloys. Trans. TMS–AIME 224 599–606.
5. Bhadeshia, H. K. D. H. 1992. Bainite in Steels Institute of Materials, London, UK.
6. Bhadeshia, H. K. D. H. 1982. Thermodynamic analysis of isothermal transformation diagrams Metal Science 16 159–165.
7. Nyström, I.; and Söderström, H. 1986. Bors roll för struktur och egenskaper i olegerade svetsgods ESAB report no. CML–86353.
8. Smith, C. S. 1948. Grains, phases and interfaces Trans. AIMME 175 15–51.
9. Babu, S. S.; and Bhadeshia, H. K. D. H. 1991. Direct study of grain boundary allotriomorphic ferrite crystallography Materials Science and Engineering A A142 209–219.
10. Snieder, G.; and Kerr, H. W. 1984. Effects of Cr and flux type on the structure and properties of HSLA steel submerged arc welds. Canadian Metall. Quart. 23 315–325.

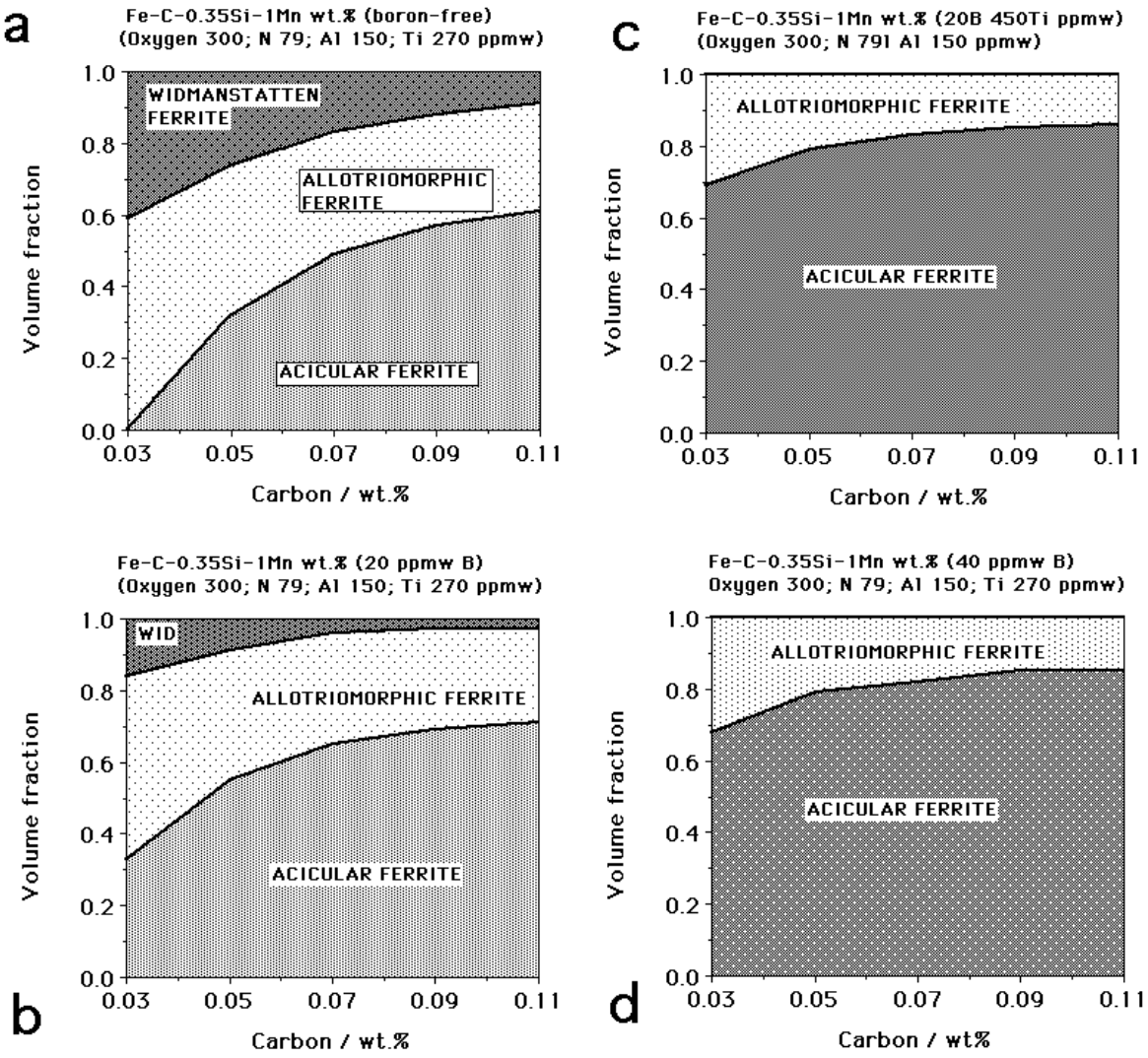

Fig. 4: Example calculations for the primary microstructure of welds a–d (Table 5).